JCTC Journal of Chemical Theory and Computation

Theoretical Investigation of the Reaction of Imidogen with Fulminic Acid

Ya-nan Xin, Min Zhao,* and Zuo-sheng Li

College of Chemistry and Chemical Engineering, Bohai University, Jinzhou, Liaoning, 121000, People's Republic of China

Wei Xiong, Xinli Song, Hua Hou, and Baoshan Wang*

College of Chemistry and Molecular Sciences, Wuhan University, Wuhan 430072, People's Republic of China

Received May 7, 2009

Abstract: The mechanism of the reaction of imidogen (NH) with fulminic acid (HCNO) has been investigated theoretically using the multiconfigurational self-consistent-field theory (MCSCF), multireference Rayleigh−Schrodinger perturbation theory (RSPT2), and coupled cluster theory (CC) along with the complete basis set extrapolations (CBS). The calculations show that the NH + HCNO reaction takes place via an N → C addition mechanism predominantly by surmounting a small barrier (ca. ∼3 kcal/mol). The adduct is HC(NH)NO in the triplet state with an exothermicity of more than 60 kcal/mol. The subsequent C−N cleavage, which is nearly barrierless, leads to HCNH and NO as the final products. This represents the most energetically favorable product channel of the title reaction. The channels leading to HCN, HNC, HNO, or HON via O- or H-migration mechanisms involve higher barriers and thus are negligible. The singlet−triplet crossing has been investigated as well for the HCNH + NO product channel by locating the conical interactions. Using transition state theory, the rate constants were predicted as a function of temperatures. It is suggested that the NH + HCNO reaction might be an alternative source for the NO regeneration under the combustion conditions. This calculation is useful to simulate experimental investigations of the NH + HCNO reaction.

I. Introduction

In contrast to its isomer isocyanic acid (HNCO), fulminic acid (HCNO) is less stable but can be synthesized and stored for brief periods in the gas phase.[1,2] The structure[1−4] and reactivity[5−11] of this molecule have attracted considerable attention both experimentally and theoretically. Under combustion conditions, HCNO is formed primarily from the acetylene oxidation followed by the HCCO + NO reaction. It plays an important role in the so-called NO-reburning process for the reduction of NO_x pollutants from the fossil-fuel emission.[11] Very recently, it has been discovered that HCNO also exists in dark clouds with an abundance of $1-5 \times 10^{-10}$ with respect to molecular hydrogen. The CH_2 + NO → HCNO + H reaction was suggested to be a key path for the formation of fulminic acid.[12]

The reactions of HCNO with a few highly reactive radicals, for example, H, O, OH, CN, NCO, etc., have been studied extensively.[5−11] Most of these reactions are significantly exothermic and relatively fast, with rate constants on the order of 10^{-11} cm^3 $molecule^{-1}$ s^{-1}. Theoretical calculations of these reactions have been reported using various quantum chemistry methods, for example, density functional theory and the coupled cluster theory.[10,11] The predicted reaction mechanisms are in agreement with the experimental observations.

$NH(X^3\Sigma^-)$ is an important radical in both combustion and atmospheric chemistry.[13−15] Although its reactivity is lower than the radicals (e.g., OH) as mentioned above, the NH

* Corresponding authors e-mail: baoshan@whu.edu.cn.

10.1021/ct9002288 CCC: $40.75
Published on Web 07/15/2009

radical can play a critical role in the NO-reburning process. In this work, the reaction of NH with HCNO is investigated theoretically using the high-level ab initio quantum chemistry methods. The theoretical data are invaluable for extending our understanding of the roles of NH and HCNO in both combustion and atmosphere. To our knowledge, the NH + HCNO reaction has not been studied either experimentally or theoretically. The present calculations might shed new light on the importance of this reaction in the gas phase.

II. Computational Methods

As a preliminary effort, the geometries of the reactants, products, intermediates, and transition states were fully optimized using the conventional B3LYP[16] and MP2[17] methods with the standard 6-311+G(d,p)[18] basis set using the Gaussian03 programs.[19] However, it was found that the single-reference wave functions are subject to severe spin contaminant. For instance, the spin expectation value $\langle S^2 \rangle$ for the association transition state TS1 is as high as 2.352 at the UMP2/6-311+G(d,p) level, whereas the correct value for the triplet is 2.0. Even for the HC(NH)NO adduct, the value of $\langle S^2 \rangle$ is 2.15. Moreover, the problem of spin contaminant cannot be conquered by using either higher order perturbation theory (e.g., MP4) or configuration interaction theory (e.g., CISD). These preliminary calculations clearly indicate that the multireference and more extensive electronic correlation methods are required to explore the energetic reaction routes of the NH + HCNO reaction.

Two high-level methods have been employed in the geometrical optimizations. The first method is the multiconfigurational self-consistent-field method (MCSCF).[20,21] The full valence active space includes 22 electrons distributed in 18 orbitals. For the sake of our computational resources, we chose a smaller active space, namely, 14 electrons in 12 orbitals, consisting of 141 760 configuration state functions (CSFs). It has been carefully checked that this active space is capable of including all the important CSFs for the stationary points (for example, see Figure S1 in the Supporting Information) and the MCSCF wave function converges to the correct ground state. The "supermolecule" approximation was used for the two fragments of the reactants and the products with a separation of 100 Å. The second method is the coupled cluster theory with single, double, and noniterative triple excitations, namely, CCSD(T).[22] For the triplet species of concern, the restricted open-shell wavefuction was used for both CCSD(T) and HF references, namely, RCCSD(T,full)-ROHF, where the term "full" means that all electrons are included in the electronic correlation calculations. The diagnostic T_1 values for the species have been monitored to be in the range 0−0.04, indicating the good quality of the RCCSD(T,full)-ROHF wave functions.[23] The 6-311+G(d,p) basis set was used for both methods. The convergency criterion requires the maximum component of the gradient to be less than 1.0×10^{-6} au in all optimization calculations.[24,25]

Harmonic vibrational frequencies for all stationary points were calculated at the same level of theory as used in the optimization [e.g., MCSCF and RCCSD(T,full)] by numerically approximating Hessian.[26,27] The minimum has all real frequencies. The transition state only involves one imaginary frequency representing the motion along the reaction coordinate. Moreover, a few intrinsic reaction coordinate (IRC)[28] calculations were carried out in order to confirm that the connections of the transition states with the designated reactants and products are valid.

On the basis of the MCSCF(14e,12o)/6-311+G(d,p)-optimized geometries, the single-point energy calculations were carried out using the multireference Rayleigh−Schrodinger perturbation theory.[29,30] More accurate multireference configuration interaction (MRCI) calculation is not affordable at present for the large (14e,12o) active space. The internally contracted version of RS2C has been chosen in this work. Moreover, a level shift of 0.2 was used in order to avoid intruder state problem in excited state calculations as suggested by Roos and Andersson.[31] Two correlation-consistent basis sets, namely, aug-cc-pVDZ and aug-cc-pVTZ,[32] were used for RS2C. The total numbers of contracted configurations are 28 709 896 and 68 432 064, respectively. The individual energies were extrapolated to the complete basis set limit (CBS) using the following expression[33]

$$E_X = E_\infty + cX^{-3} \quad (X = 2, 3) \tag{1}$$

where X represents the cardinal number X of the aug-cc-pVXZ basis sets.

On the basis of the RCCSD(T,full)/6-311+G(d,p)-optimized geometries, further RCCSD(T,full) single-point calculations were done using the aug-cc-pVDZ and aug-cc-pVTZ basis sets. Moreover, an additional ROHF single-point energy was obtained using the aug-cc-pVQZ basis set. Then, the full coupled-cluster energy (FCC) was calculated using the following expressions:[34,35]

$$E(\mathrm{FCC}) = E_\infty[\mathrm{CCSD(T)}] + 1/5\Delta E^T_{\mathrm{aug-cc-pVTZ}} \tag{2}$$

$$E_\infty[\mathrm{CCSD(T)}] = E_\infty(\mathrm{HF}) + \Delta E_\infty[\mathrm{CCSD(T)}] \tag{3}$$

$$E_X(\mathrm{HF}) = E_\infty(\mathrm{HF}) + a\exp(-bX) \tag{4}$$

$$\Delta E_X[\mathrm{CCSD(T)}] = \Delta E_\infty[\mathrm{CCSD(T)}] + cX^{-3} \tag{5}$$

In addition, the extrapolation scheme developed by Truhlar was used for the purpose of comparison and cross-validation of the CBS extrapolations, viz.[36]

$$E_\infty[\mathrm{CCSD(T)}] = \frac{3^\alpha E_{\mathrm{HF},3} - 2^\alpha E_{\mathrm{HF},2}}{3^\alpha - 2^\alpha} + \frac{3^\beta E_{\mathrm{corr},3} - 2^\beta E_{\mathrm{corr},2}}{3^\beta - 2^\beta} \tag{6}$$

where $\alpha = 3.4$ and $\beta = 2.4$. All of the above ab initio calculations were carried out using the Molpro2006.1 program.[37]

III. Results and Discussion

The optimized geometries of the reactants, products, intermediates (INT), and transition states (TS) at the MCSCF(14e,12o) and RCCSD(T,full) levels of theory are shown comparatively in Figure 1. The key energetic reaction routes are shown

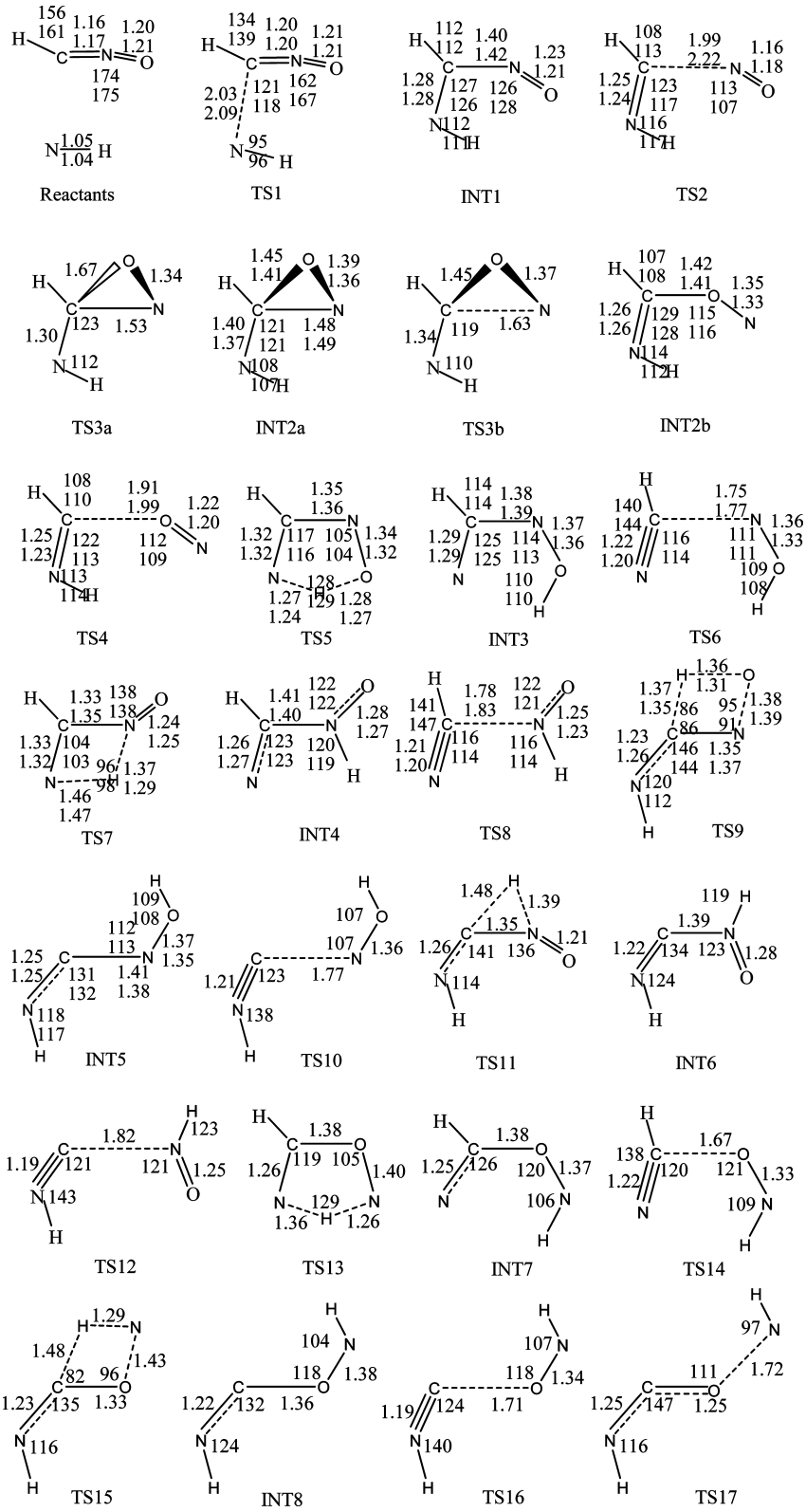

Figure 1. Geometries of the transition states (TS) and intermediates (INT) involved in the NH + HCNO reaction. Bond distances are in Ångstroms, and bond angles are in degrees. Upper entries: the MCSCF(14e,12o)/6-311+G(d,p)-optimized parameters. Lower entries: the RCCSD(T,full)/6-311+G(d,p)-optimized parameters.

schematically in Figure 2. The zero-point energies (ZPE) and relative energies for all stationary points are summarized in Table 1. More data including vibrational frequencies (Table S1 in the Supporting Information) and full reaction mechanisms calculated at the G4//MP2(full)/6-311+G(d,p) level (Figure S2 in the Supporting Information) are deposited as Supporting Information.

The effect of the sizes of the basis sets on the geometrical parameters was carefully checked as well using 6-311++G(2d,2p), 6-311++G(3df,3pd), aug-cc-pVDZ, and aug-cc-pVTZ basis

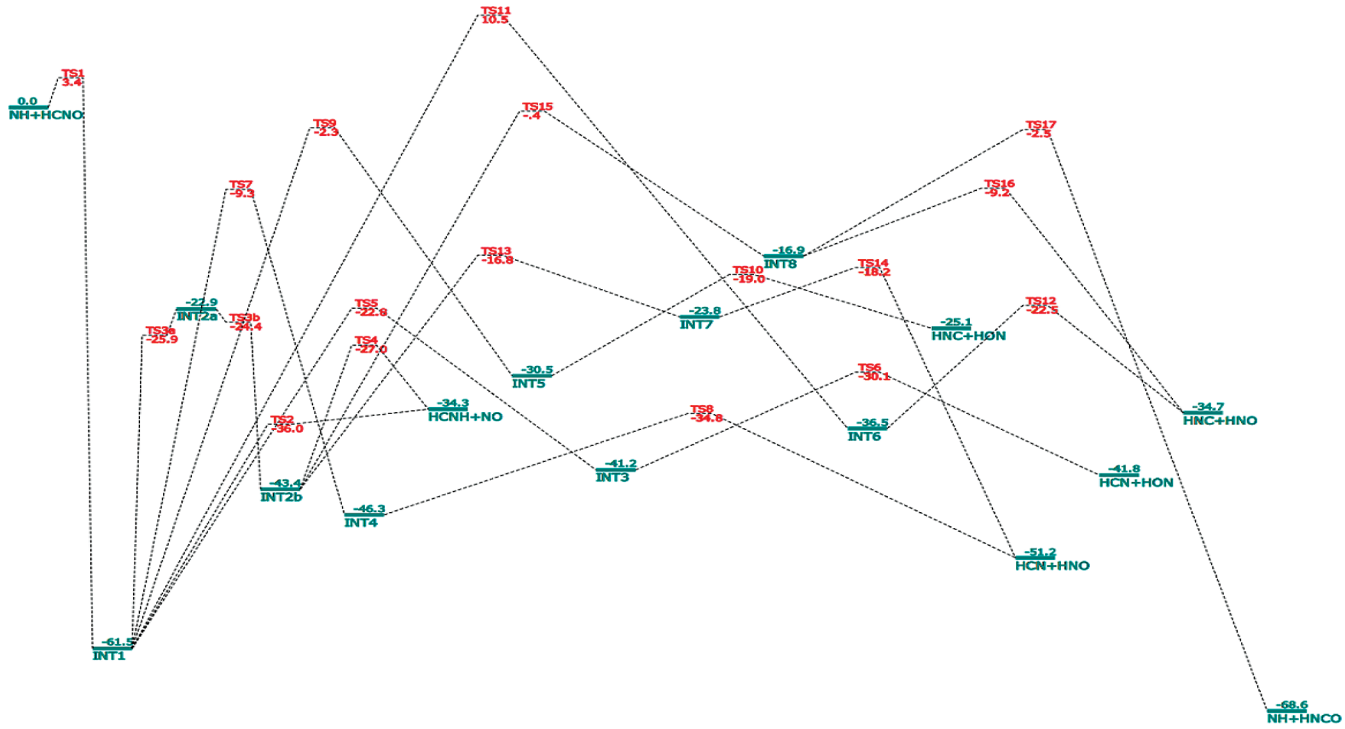

Figure 2. Energetic reaction routes of the NH + HCNO reaction. The energies calculated at the RS2C/CBS//MCSCF(14e,12o)/6-311+G(d,p) level are shown in units of kcal/mol.

sets for the association transition state (TS1) and intermediate (INT1). These data are shown in the Supporting Information (Tables S2 and S3). It is evident that the basis set employed in this work, i.e., 6-311+G(d,p), is adequate for the geometrical optimizations.

The geometry of fulminic acid is still uncertain. It was suggested by the high-level ab initio calculations that HCNO has a bent geometry, but the collinear geometry is only a few wavenumbers higher in energy.[2−4] Our results obtained at both MCSCF and RCCSD(T) levels are in good agreement with previous calculations. Moreover, the RCCSD(T) vibrational frequencies are in good agreement with the experimental infrared measurements (see Table S1 in the Supporting Information).[1] In fact, HCNO can be seen as a resonant structure between H−C≡N−O and H−C═N═O.

There are four possible reaction sites while NH is approaching toward the H, C, N, and O atoms of HCNO. As shown in Figure S2 in the Supporting Information, the H abstraction and the N- and O-addition pathways are endothermic and involve significant barriers. Therefore, they are negligible. In the following section, only the C-addition reaction mechanism will be discussed in detail. Note that most of the stationary points are shown to be planar structures and possess $^3A''$ electronic states in the C_s symmetry, in accordance with the adiabatic correlation asymptote of $NH(X^3\Sigma^-) + HCNO(X^1A')$.

1. N−C Addition Path. The association reaction occurs between the N atom of NH and the C atom of HCNO. The singly occupied p orbital of NH is approaching the Π orbitals of HCNO to form the CN bond (see Figure S1 in the Supporting Information). The adduct is denoted as INT1. In view of the spin densities, the Π orbital of HCNO is broken totally because the two radical centers move to N and O atoms, respectively. The newly formed CN bond exhibits double-bonding character, and the other C−N bond is a single bond. The addition step is highly exothermic by more than 60 kcal/mol.

The transition state for association is shown as TS1 in Figure 1. The Π orbital of HCNO is only slightly affected by the approaching p orbital of the N atom in NH. Evidently, it is an early barrier. The approaching C···N distance is about 0.8 Å longer than that in INT1. Note that TS1 is the only true transition state for the association even though the adduct INT1 has an isomer with the *cis*-HCNO conformation. The geometrical parameters obtained at the MCSCF level are in reasonable agreement with those at RCCSD(T) level, although RCCSD(T) tends to give an earlier transition state.

It is extremely difficult to calculate the barrier height for such a loose barrier. At the RS2C/CBS//MCSCF(14e,12o)/6-311+G(d,p) level, the classical barrier height (e.g., without ZPE) becomes negative, namely, −3.4 kcal/mol. However, at the FCC/CBS//RCCSD(T,full)/6-311+G(d,p) level, the classical barrier is 1.4 kcal/mol. If the RCCSD(T,full)/6-311+G(d,p)-optimized geometrical parameters were used, the calculated RS2C/CBS barrier height increases to −1.5 kcal/mol. The barrier height seems to be very sensitive to the geometry of the transition state.

In order to clarify what happens in these calculations, we performed an IRC calculation of TS1 at the MCSCF(6e,6o)/6-311+G(d,p) level of theory. For every point along the obtained minimum energy reaction path, we calculated the high-level energies using RS2C, CASMP2,[38] MRCI, and MRCI+Q methods[39,40] based on the MCSCF(6,6) configurations. The results are shown in Figure 3. It is obvious that the position of the barrier depends on the levels of theory.

Table 1. Relative Energies (in kcal/mol) for the Important Species Involved in the NH + HCNO Reaction[a]

species	ΔZPE_{MCSCF}	ΔE_{MCSCF}	ΔE_{RS2C}	$\Delta ZPE_{RCCSD(T)}$	T_1[f]	$\Delta E_{RCCSD(T)}$	ΔE_{FCC}	$\Delta E_{FCC\text{-}Truhlar}$
TS1	2.5	2.8	−3.4	2.1	0.024	4.1	1.4	1.4
			−1.5[b]					
			0.4[c]					
			1.3[d]					
			2.0[e]					
INT1	7.7	−43.0	−68.8	7.0	0.025	−63.4	−68.0	−67.5
TS2	4.7	−15.5	−40.3	3.2	0.023	−39.0	−39.4	−38.6
HCNH + NO	2.9	−44.5	−36.9	2.4		−41.4	−38.4	−37.2
TS3a	5.1	−10.0	−31.0					
INT2a	6.0	−12.2	−28.6	5.6	0.026	−26.8	−29.6	−29.7
TS3b	5.3	−8.8	−29.4					
INT2b	7.0	−39.1	−50.1	6.4	0.019	−50.1	−50.9	−50.6
TS4	4.0	−14.1	−30.7	3.3	0.034	−28.8	−30.7	−29.8
TS5	2.9	4.6	−25.3	2.9	0.027	−18.8	−24.9	−24.5
INT3	5.9	−26.8	−46.7	5.7	0.025	−42.9	−45.4	−44.7
TS6	4.5	−18.2	−34.3	3.7	0.020	−29.9	−32.4	−32.0
HCN + NOH	2.6	−48.8	−44.1	2.2		−46.8	−42.0	−41.3
TS7	3.0	18.7	−12.0	2.9	0.034	−1.8	−7.9	−7.5
INT4	6.4	−26.2	−52.3	6.2	0.025	−49.1	−52.2	−51.8
TS8	3.5	−19.9	−37.9	2.9	0.039	29.8	−32.4	−32.1
HCN + HNO	2.3	−54.4	−53.2	1.9		−51.7	−50.6	−50.1
TS9	2.5	30.4	−4.5	2.2	0.035	4.4	−0.4	−0.3
INT5	6.4	−10.4	−36.5	5.5	0.027	−31.6	−35.5	−35.0
TS10	4.2	−0.8	−22.8		0.027		−17.8[g]	−17.3[g]
HNC + HON	2.4	−26.8	−27.2	1.9		−31.5	−26.4	−25.5
TS11	1.8	62.8	9.0					
INT6	6.8	−18.6	−43.0					
TS12	4.2	−0.4	−26.4					
HNC + HNO	2.1	−33.5	−36.4					
TS13	3.1	5.7	−19.6	3.0	0.031	−14.9	−17.6	−17.5
INT7	6.1	−19.2	−29.6	5.1	0.021	−28.6	−30.9	−30.9
TS14	3.8	−7.3	−21.6	3.3	0.039	−16.9	−18.8	−18.4
TS15	2.6	32.4	−2.7					
INT8	5.8	−4.9	−22.3					
TS16	3.7	15.5	−12.6					
TS17	2.9	24.1	−5.0					
NH + HNCO	1.8	−69.6	−70.0					

[a] All energies are calculated with respect to the NH + HCNO asymptote. ΔZPE_{MCSCF} and ΔE_{MCSCF}: zero-point energies and electronic energies calculated at the MCSCF(14e,12o)/6-311+G(d,p) level of theory. ΔE_{RS2C}: energies calculated at the RS2C/CBS//MCSCF(14e,12o)/6-311+G(d,p) level of theory. $\Delta ZPE_{RCCSD(T)}$ and $\Delta E_{RCCSD(T)}$: zero-point energies and electronic energies calculated at the RCCSD(T,full)/6-311+G(d,p) level of theory. ΔE_{FCC} and $\Delta E_{FCC\text{-}Truhlar}$: energies calculated at the extrapolated full coupled-cluster theory using expressions E4 and E5, respectively. [b] Calculated at the RS2C/CBS//RCCSD(T,full)/6-311+G(d,p) level. [c] Calculated at the RS2C/CBS//MRCI(6e,6o)/6-311+G(d,p) level. [d] Calculated at the RS2C/CBS//MRCI(6e,6o)+Q/6-311+G(d,p) level. [e] Calculated at the RS2C/CBS//RS2C(6e,6o)/6-311+G(d,p) level. [f] T_1 diagnostic values calculated at the RCCSD(T,full)/AVTZ level. [g] The RCCSD(T,full)/6-311+G(d,p) optimization cannot converge. The energies were calculated using the MCSCF(14e,12o)/6-311+G(d,p)-optimized geometry.

At the RS2C/CBS level, the transition state occurs at $R(C\cdots N) = 2.25$ Å, which is significantly longer than that obtained at the MCSCF level. This explains why the RS2C-calculated barrier height at the MCSCF-optimized geometry is even negative. Both MRCI and MRCI+Q methods predict longer $R(C\cdots N)$ as well. It implies that besides the nondynamical effect, the dynamical electronic correlation is also important in the determination of TS1. The noncontinuous energies at the CASMP2 level are due to the so-called "state intrude" problem. This verifies that the shift parameters in our RS2C calculations are important to obtain reasonable energies. The RS2C/CBS-calculated barrier heights are 0.4, 1.3, and 2.0 kcal/mol using the MRCI, MRCI+Q, and RS2C maxima, respectively. These values are in reasonable with those obtained at the FCC/CBS//RCCSD(T,full)/6-311+G(d,p) levels. With the above investigations, we feel confident that the barrier for the association path does exist, although it is very low. The classical barrier should be in the range 1−2 kcal/mol. After the ZPE correction, the barrier height is estimated to be 3.5 kcal/mol.

2. INT1 → HCNH + NO Dissociation Path. As mentioned above, due to the addition of NH to the C atom of HCNO, the CN bond is significantly stretched to 1.4 Å. Meanwhile, the association results in plenty of energy to INT1 and the C−N bond is readily broken to produce HCNH and NO.

We found a transition state TS2 for this CN bond scission process. As shown in Figure 1, TS2 is a very loose transition state. The C···N distance is nearly 2.0 Å at the MCSCF level, and it is even longer if the dynamical electronic correlation has been included using the RCCSD(T) method. In fact, the energy of TS2 is somewhat lower than that of the products at both RS2C/CBS and FCC/CBS levels. Apparently, C···N fission would occur without any well-defined transition state. The formation of HCNH + NO is highly exothermic by 36 kcal/mol.

Note that INT1 has a conformer with the *cis*-HCNO geometry. Its energy is ∼1 kcal/mol higher than that of INT1. Interestingly, the C···N fission of the *cis*-INT1 does involve

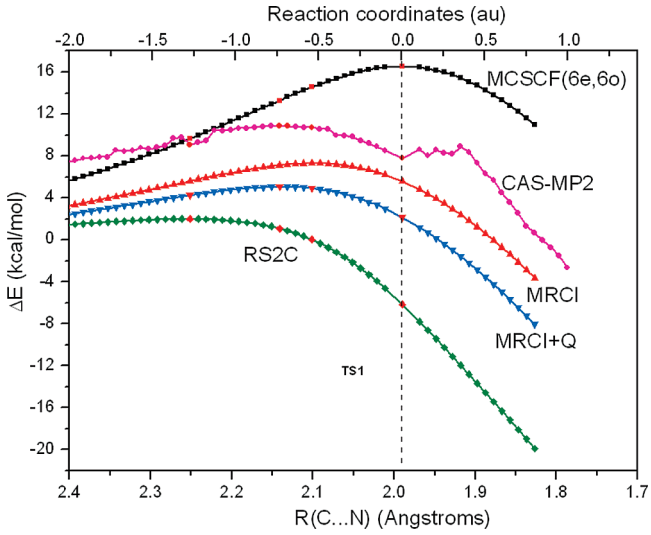

Figure 3. Minimum energy path for the association reaction of NH with HCNO. All relative energies (in kcal/mol) are calculated at the MCSCF(6e,6o)/6-311+G(d,p) level with respect to the NH + HCNO asymptote. On the basis of the geometries of each point along the MEP, the single-point energies were calculated using the CASMP2, MRCI, and RS2C methods with the aug-cc-pVDZ and aug-cc-pVTZ basis sets and then the energies were extrapolated to the complete basis set limit using eq 1. The term "Q" in the MRCI+Q method means the empirical Davidson correction to the MRCISD energy.

a well-defined barrier whose energy is about 1 kcal/mol higher that that of the products.

3. O-Rearrangement Channel Starting from INT1. Since the ground state of NH has $^3\Sigma^-$ symmetry, the NH + HCNO asymptote adiabatically correlates to the $^3A''$ electronic state in the C_s point group. However, an oxygen-shift reaction route exists starting from INT1($^3A''$) by breaking the C_s symmetry. The transition state is TS3a as shown in Figure 1. The terminal O atom is bent to the central C atom, forming a three-memebered cyclic structure, INT2a. Interestingly, the classical barrier for this process is only 38 kcal/mol, which is even lower than those for the H-shift paths as will be discussed below. TS3a is the second lowest barrier in the INT1 reaction. However, the CON ring in INT2a is very unstable. The CN bond is readily broken to form a new planar intermediate, namely, INT2b. In comparison with INT1, the two singly occupied electrons in INT2b are localized on the terminal N atom. The energy of INT2b is 18 kcal/mol higher than that of INT1. The CO bond cleavage of INT2b is undergone via TS4 with the formation of HCNH + NO. TS4 appears to be a tighter barrier than TS2, although their geometrical parameters are similar. As a result, TS4 is a well-defined transition state. Its energy is about 7 kcal/mol higher than that of the products.

4. Singlet−Triplet Crossing for the HCNH + NO Channel. The reaction mechanism for the HCNH(X^2A') + NO($X^2\Pi$) channel could be more complicated if the surface crossing was considered because this channel does correlate adiabatically with both triplet and singlet surfaces in view of the two doublet product molecules. Using the state-averaged MCSCF(14e,12o)/6-311+G(d,p) method, the conical interactions between triplet and singlet surfaces relevant to the NH + HCNO → HCNH + NO reaction have been studied. The energetic profiles are shown in Figure 4.

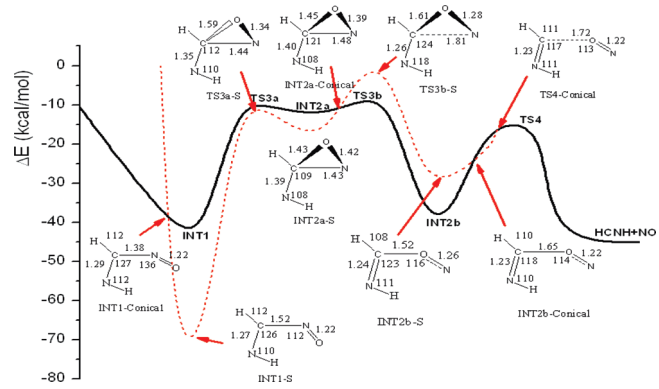

Figure 4. Singlet−triplet crossings on the potential-energy surface of the NH + HCNO → HCNH + NO reaction. Solid line: triplet. Dashed line: singlet. The energies (in kcal/mol) were calculated at the state-average MCSCF(14e,12o)/6-311+G(d,p) level of theory with respect to the reactant asymptote. The geometries of the singlet species and the conical interactions are shown. Bond distances are in Ångstroms, and angles are in degrees.

The open-shell singlet INT1-S was first located as shown in Figure 4. There are two differences between INT1 and INT1-S, namely, the CN bond length and the CNO bond angle. INT1-S has a longer CN bond but much smaller CNO angle. In terms of energy, INT1-S is much more stable than the triplet INT1. The conical interaction between INT1-S and INT1 is shown as INT1-conical in Figure 4. It has the same CN bond length with INT1, and its energy is close to INT1 as well. Apparently, the S−T crossing might occur through changing the CNO angles.

Through the potential-energy scan of the CN bond distances it is found that the CN bond fission of INT1-S is barrierless, leading to HCNH + NO directly without any crossing with the triplet path. The O-migration mechanism is complex. As shown in Figure 4, the first part of the reaction path involves singlet TS3a-S and INT2a-S. Later, there is a crossing between INT2a and INT2a-S via INT2a-conical, whose geometry and energy are nearly the same as INT2a. TS3b-S is a much higher barrier, and the breaking C···N bond is much longer than that of TS3b. The intermediate INT2b-S has a similar geometry with INT2b except for the longer CO bond. As the CO bond is stretching, there are two crossing intersections between triplet and singlet, namely, INT2b-conical and TS4-conical. However, we cannot obtain reasonable energetic profiles on the singlet surface when the CO distances are elongated further because the MCSCF calculations cannot converge to the correct electronic states. Probably, the dissociation asymptote of INT2b corresponds to the electronically excited products.

At present, we are unable to calculate the singlet−triplet transition probability. However, it is probably small as is typical of a spin forbidden transition in the absence of heavy elements. The most energetically favorable reaction path, namely, NH + HCNO → TS1 → INT1 → TS2 → HNCH + NO, could be a reasonable mechanistic representation for

the NH + HCNO reaction and will be used for the subsequent kinetic calculation.

5. H-Shift Reaction Paths from INT1. There are a few H-shift reaction pathways starting from either INT1 or INT2b via five-, four-, or three-membered ring transition states. Although all these channels involve significant barriers, the energies of transition states are still lower than that of the reactant asymptote. It is conceivable that the 1,4-H-shift path has the lowest barrier, forming INT3 via transition state TS5. Subsequently, the C−N bond cleavage produces HCN and HON. It is worth noting that HON is in its excited triplet state rather than the singlet because of the spin conservation.

Transition state TS7 is for the four-center 1,3-H-shift path, leading to INT4. The energy of TS7 is more than 10 kcal/mol higher than that of TS5. However, INT4 is more stable than INT3. The CN bond fission leads to HCN and triplet HNO via TS8. It is noted that HCN + HNO is the most exothermic channel for the NH + HCNO reaction, even though HNO is produced in the triplet excited state. The other four-center transition state is TS9, showing a H-shift pathway from C to O. The intermediate INT5 can decompose to HNC and HON via TS10. Another H-shift starting from INT1 occurs via TS11, which is a three-center structure. The energy of TS11 is about 10 kcal/mol higher than that of the NH + HCNO asymptote. Therefore, this H-shift path could be unimportant, although intermediate INT6 is very stable in view of its low energy and the decomposition barrier (TS12) for the HNC + HNO channel is relatively low.

There are two H-shift pathways starting from INT2b. 1,4-N,N shift occurs via TS13, whose energy is about 10 kcal/mol higher than that for the decomposition of INT2b. The intermediate INT7 decomposes to HCN and HNO via TS14. The other H-shift path involves a more significant barrier since TS15 is a four-center transition state. However, the intermediate INT8 still lies below the NH + HCNO asymptote. The CO bond cleavage of INT8 produces HNC and HNO via TS16. The NO bond stretching of INT8 leads to NH and HCNO, which is the most stable species in the [H,C,N,O] system.

Although there are many low-energy reaction pathways in the NH + HCNO reaction, the barriers are well separated. In conclusion, it appears to have a relatively simple reaction mechanism. The major mechanism can be simplified as follows:

$$\mathrm{NH + HCNO \rightarrow TS1 \rightarrow INT1 \rightarrow TS2 \rightarrow HCNH + NO} \quad \text{(R1)}$$

$$\rightarrow \mathrm{TS3 \rightarrow INT2 \rightarrow TS4 \rightarrow HCNH + NO} \quad \text{(R2)}$$

Evidently, HCNH and NO should be the major products of the reaction. Another channel starting from INT1, namely,

$$\mathrm{INT1 \rightarrow TS5 \rightarrow INT3 \rightarrow TS6 \rightarrow HCN + HON} \quad \text{(R3)}$$

could be a very minor path under the specific conditions.

6. Temperature- and Pressure-Dependent Rate Constants. For the sake of completeness, the whole mechanism as shown in Figure 2 has been employed for the kinetic analysis using the conventional transition state theory and the multichannel Rice−Ramsperger−Kassel−Marcus theory (RRKM). The algebraic expressions of the RRKM calculations have been well developed by us and successfully used for kinetic estimates of many radical reactions.[41,42] Formulas and parameters in the kinetic calculation are deposited in the Supporting Information (see Note S1) in detail. Briefly, the rigid rotor harmonic oscillator (RRHO) approximation was used for all stationary points at the *E*-resolved level. The transition states were treated nonvariationally, and the tunneling effect has been neglected. In the calculation of the pressure dependence, N_2 was used as the bath gas using Troe's weak-collision model.[43] It is worth noting that the present rate constants are only rough estimates in view of the uncertainty of the theoretical barrier heights and various approximations used in the transition state theory and master equation analysis.

Since both RS2C/CBS//MCSCF(14e,12o)/6-311+G(d,p) and FCC/CBS//RCCSD(T,full)/6-311+G(d,p) methods give similar energetic and geometrical data for the key stationary points (e.g., the intermediates and transition states in channels R1−R3), the ab initio data calculated at the RS2C/CBS//MCSCF(14e,12o)/6-311+G(d,p) level of theory were used to predict the rate constants as a function of temperature. It is worth noting that HCNO was considered to be a collinear species.

It appears that the NH + HCNO reaction is pressure independent. The association reaction is highly exothermic. The reaction well INT1 is as deep as 61 kcal/mol, and the decomposition of INT1 to form HCNH and NO is a nearly barrierless process. This feature of the potential-energy surface implies that the energy-rich intermediate INT1 has little chance to be quenched by the bath gases except for at extremely high pressures. Our transition state theory calculation does verify this fact (e.g., $P > 10^6$ Torr of bath gas is required to produce significant INT1).

The temperature-dependent rate constants for the NH + HCNO reaction in the temperature range 250−3000 K are shown in Figure 5. The HCNH + NO channel is always the dominant path, and the other product channels contribute less than 1%. The overall rate constants show positive temperature dependence in accordance with the small barrier at the entrance. Moreover, a typical non-Arrhenius curvature is observed. The rate constants were least-squares fitted using an empirical three-parameter expression as follows

$$k(T = 250 - 3000\ \mathrm{K}) = 1.81 \times 10^{-13}(T/300)^{1.97} e^{-1.39\ \mathrm{kcal/mol}/RT} \quad (7)$$

in units of $\mathrm{cm^3\ molecule^{-1}\ s^{-1}}$. As shown in Figure 5, the fitting to the low- and high-temperature ranges separately shows better result, namely,

$$k(T < 1000\ \mathrm{K}) = 3.56 \times 10^{-13}(T/300)^{1.67} e^{-1.98\ \mathrm{kcal/mol}/RT} \quad (8)$$

$$k(T > 1000\ \mathrm{K}) = 1.72 \times 10^{-13}(T/300)^{1.98} e^{-1.32\ \mathrm{kcal/mol}/RT} \quad (9)$$

At lower temperatures, the NH + HCNO reaction occurs slowly. Under the high-temperature combustion conditions, the reaction becomes fast. For example, the rate constant is

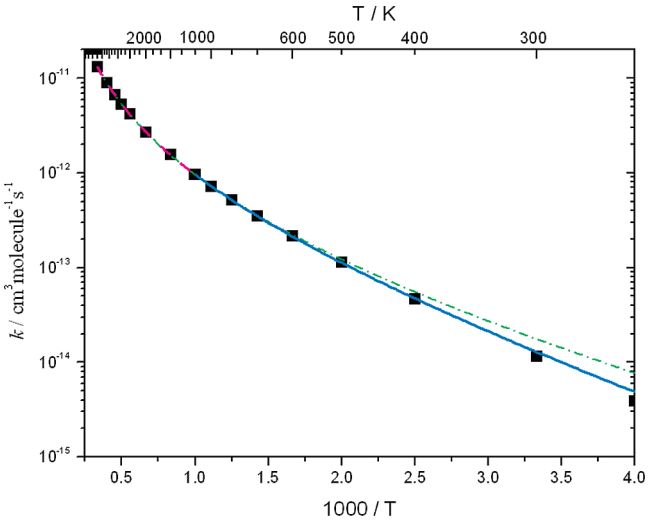

Figure 5. Overall rate constants for the NH + HCNO reaction as a function of temperatures calculated using the RS2C/CBS//MCSCF(14e,12o)/6-311+G(d,p) ab initio data. Solid line: best fit in the range 250−1000 K. Dashed line: best fit in the range 1000−3000 K. Dash-dotted line: best fit to the entire data.

5.33×10^{-12} cm^3 molecule^{-1} s^{-1} at 2000 K and increases to be twice that at 3000 K. More significantly, the major reaction products include both HCNH and NO. It implies that the NH + HCNO reaction might be a potentially important source of NO regeneration under the combustion conditions. On the other hand, decomposition of the HCNH radical into either H + HCN or H_2 + CN is also energetically feasible because of the significant energy released in the HCNH + NO channel.[44,45] Experimental study of the NH + HCNO reaction might be interesting in view of the present theoretical findings.

IV. Conclusions

In this work, two types of high-level ab initio methods, namely, multireference Rayleigh−Schrodinger perturbation theory based on the multiconfigurational self-consistent-field theory and the coupled cluster theory along with the complete basis set extrapolations, were used to explore the mechanism of the NH + HCNO reaction. On the triplet potential-energy surface, a small barrier of about 3 kcal/mol exists for the C···N association path. The association step is highly exothermic by more than 60 kcal/mol, and the intermediate HC(NH)NO can decompose rapidly to form HCNH and NO radicals, which are the dominant products. Another two routes for the HCNH + NO production include the symmetry-breaking O-rearrangement process and the singlet−triplet surface crossing path. Other products such as HCN and HNO are shown to be unimportant.

The rate constants for the NH + HCNO reaction were predicted on the basis of the ab initio data. The rate constants are positively temperature dependent and show non-Arrhenius behavior. It is shown that the NH + HCNO reaction is fast under high-temperature combustion conditions. Moreover, the rapid production of NO and HCNH (may decompose to H + HCN or CN + H_2) implies that the NH + HCNO reaction might play an important role in the NO-reburning process.

Acknowledgment. This work was supported by NSFC (no. 20673079, 20603025).

Supporting Information Available: Figures of the active spaces in the MCSCF calculations for some key species involved in the NH + HCNO reaction and G4//MP2(full)/6-311+G(d,p) calculated potential-energy surface for the NH + HCNO reaction. Tables of the MCSCF(14e,12o)/6-311+G(d,p) and RCCSD(T,full)/6-311+G(d,p) calculated harmonic vibrational frequencies and optimized geometries for TS1 and INT1 with different basis sets. Note S1 lists the details for the kinetic calculation. This material is available free of charge via the Internet at http://pubs.acs.org.

References

(1) Beck, D. W.; Feldl, K. *Angew. Chem., Int. Ed.* **1966**, *5*, 722.

(2) Schuurman, M. S.; Muir, S. R.; Allen, W. D.; Schaefer, H. F., III. *J. Chem. Phys.* **2004**, *120*, 11587.

(3) Nguyen, M. T.; Pierloot, K.; Vanquickenborne, L. G. *Chem. Phys. Lett.* **1991**, *181*, 83.

(4) Koput, J.; Winnewisser, B. P.; Winnewisser, M. *Chem. Phys. Lett.* **1996**, *255*, 357.

(5) Zhang, W. C.; Du, B. N.; Feng, C. J. *Chem. Phys. Lett.* **2007**, *442*, 1.

(6) Li, B. T.; Zhang, J.; Wu, H. S.; Sun, G. D. *J. Phys. Chem. A* **2007**, *111*, 7211.

(7) Feng, W. H.; Hershberger, J. F. *J. Phys. Chem. A* **2007**, *111*, 3831.

(8) Feng, W. H.; Hershberger, J. F. *J. Phys. Chem. A* **2006**, *110*, 12184.

(9) Grimme, S.; Muck-Lichtenfeld, C.; Wurthwein, E. U.; Ehlers, A. W.; Goumans, T. M.; Lammertsma, K. *J. Phys. Chem. A* **2006**, *110*, 2583.

(10) Feng, W. H.; Hershberger, J. F. *Chem. Phys. Lett.* **2008**, *457*, 307.

(11) Miller, J. A.; Klippenstein, S. J.; Glarborgb, P. *Combust. Flame* **2003**, *135*, 357.

(12) Marcelino, N.; Cernicharo, J.; Tercero, B.; Roueff, E. *Astrophys. J.* **2009**, *690*, L27.

(13) Quandt, R. W.; Hershberger, J. F. *J. Phys. Chem.* **1995**, *99*, 16939.

(14) Romming, H. J.; Wagner, H. G. *Symp. Int. Combust. Proc.* **1996**, *26*, 559.

(15) Mullen, C.; Smith, M. A. *J. Phys. Chem. A* **2005**, *109*, 1391.

(16) Becke, A. D. *J. Chem. Phys.* **1993**, *98*, 5648.

(17) Moller, C.; Plesset, M. S. *Phys. Rev.* **1934**, *46*, 618.

(18) Krishnan, R.; Binkley, J. S.; Seeger, R.; Pople, J. A. *J. Chem. Phys.* **1980**, *72*, 650.

(19) Frisch, M. J.; Trucks, G. W.; Schlegel, H. B.; Scuseria, G. E.; Robb, M. A.; Cheeseman, J. R.; Montgomery, J. A., Jr.; Vreven, T.; Kudin, K. N.; Burant, J. C.; Millam, J. M.; Iyengar, S. S.; Tomasi, J.; Barone, V.; Mennucci, B.; Cossi, M.; Scalmani, G.; Rega, N.; Petersson, G. A.; Nakatsuji, H.; Hada, M.; Ehara, M.; Toyota, K.; Fukuda, R.; Hasegawa, J.;

Ishida, M.; Nakajima, T.; Honda, Y.; Kitao, O.; Nakai, H.; Klene, M.; Li, X.; Knox, J. E.; Hratchian, H. P.; Cross, J. B.; Bakken, V.; Adamo, C.; Jaramillo, J.; Gomperts, R.; Stratmann, R. E.; Yazyev, O.; Austin, A. J.; Cammi, R.; Pomelli, C.; Ochterski, J. W.; Ayala, P. Y.; Morokuma, K.; Voth, G. A.; Salvador, P.; Dannenberg, J. J.; Zakrzewski, V. G.; Dapprich, S.; Daniels, A. D.; Strain, M. C.; Farkas, O.; Malick, D. K.; Rabuck, A. D.; Raghavachari, K.; Foresman, J. B.; Ortiz, J. V.; Cui, Q.; Baboul, A. G.; Clifford, S.; Cioslowski, J.; Stefanov, B. B.; Liu, G.; Liashenko, A.; Piskorz, P.; Komaromi, I.; Martin, R. L.; Fox, D. J.; Keith, T.; Al-Laham, M. A.; Peng, C. Y.; Nanayakkara, A.; Challacombe, M.; Gill, P. M. W.; Johnson, B.; Chen, W.; Wong, M. W.; Gonzalez, C.; Pople, J. A. *Gaussian03*, Revision D.01; Gaussian, Inc.: Wallingford, CT, 2004.

(20) Werner, H.-J.; Knowles, P. J. *J. Chem. Phys.* **1985**, *82*, 5053.

(21) Knowles, P. J.; Werner, H.-J. *Chem. Phys. Lett.* **1985**, *115*, 259.

(22) Knowles, P. J.; Hampel, C.; Werner, H.-J. *J. Chem. Phys.* **1993**, *99*, 5219Erratum: Knowles, P. J.; Hampel, C.; Werner, H.-J. *J. Chem. Phys.* **2000**, *112*, 3106.

(23) Lee, T. J.; Taylor, P. R. *Int. J. Quantum Chem. Symp.* **1989**, *23*, 199.

(24) Busch, T.; Degli-Esposti, A.; Werner, H.-J. *J. Chem. Phys.* **1991**, *94*, 6708.

(25) Eckert, F.; Pulay, P.; Werner, H.-J. *J. Comput. Chem.* **1997**, *18*, 1473.

(26) Rauhut, G.; El-Azhary, A.; Eckert, F.; Schumann, U.; Werner, H.-J. *Spectrochim. Acta* **1999**, *55*, 651.

(27) Hrenar, T.; Rauhut, G.; Werner, H.-J. *J. Phys. Chem. A* **2006**, *110*, 2060.

(28) Eckert, F.; Werner, H.-J. *Theor. Chem. Acc.* **1998**, *100*, 21.

(29) Werner, H.-J. *Mol. Phys.* **1996**, *89*, 645.

(30) Celani, P.; Werner, H.-J. *J. Chem. Phys.* **2000**, *112*, 5546.

(31) Roos, B. O.; Andersson, K. *Chem. Phys. Lett.* **1995**, *245*, 215.

(32) Dunning, T. H., Jr. *J. Chem. Phys.* **1989**, *90*, 1007.

(33) Helgaker, T.; Klopper, W.; Koch, H.; Noga, J. *J. Chem. Phys.* **1997**, *106*, 9639.

(34) Feller, D. *J. Chem. Phys.* **1993**, *98*, 7059.

(35) He, H.; He, Z.; Cremer, D. *Chem. Phys. Lett.* **2000**, *317*, 535.

(36) Truhlar, D. G. *Chem. Phys. Lett.* **1998**, *294*, 45.

(37) Werner, H.-J.; Knowles, P. J.; Lindh, R.; Manby, F. R.; Schrutz, M.; Celani, P.; Korona, T.; Mitrushenkov, A.; Rauhut, G.; Adler, T. B.; Amos, R. D.; Bernhardsson, A.; Berning, A.; Cooper, D. L.; Deegan, M. J. O.; Dobbyn, A. J.; Eckert, F.; Goll, E.; Hampel, C.; Hetzer, G.; Hrenar, T.; Knizia, G.; Koppl, C.; Liu, Y.; Lloyd, A. W.; Mata, R. A.; May, A. J.; McNicholas, S. J.; Meyer, W.; Mura, M. E.; Nicklass, A.; Palmieri, P.; Pfluger, K.; Pitzer, R.; Reiher, M.; Schumann, U.; Stoll, H.; Stone, A. J.; Trarroni, R.; Thorsteinsson, T.; Wang, M.; Wolf, A. *MOLPRO2006.1*, *A package of ab initio programs*; University College Cardiff Consultants Ltd: Cardiff, U.K., 2006; http://www.molpro.net.

(38) McDouall, J. J.; Peasley, K.; Robb, M. A. *Chem. Phys. Lett.* **1988**, *148*, 183.

(39) Werner, H.-J.; Knowles, P. J. *J. Chem. Phys.* **1988**, *89*, 5803.

(40) Knowles, P. J.; Werner, H.-J. *Chem. Phys. Lett.* **1988**, *145*, 514.

(41) Hou, H.; Wang, B. *J. Chem. Phys.* **2007**, *127*, 054306.

(42) Hou, H.; Li, A.; Hu, H.; Li, Y.; Li, H.; Wang, B. *J. Chem. Phys.* **2005**, *112*, 224304.

(43) Troe, J. *J. Chem. Phys.* **1977**, *66*, 4745.

(44) Metropoulos, A.; Thompson, D. L. *J. Mol. Struct: THEOCHEM* **2007**, *822*, 125.

(45) Horst, M. A.; Schatz, G. C.; Harding, L. B. *J. Chem. Phys.* **1996**, *105*, 558.

CT9002288